j mater res technol. 2020;9(6):12917–12925

Available online at www.sciencedirect.com

jmr&t
Journal of Materials Research and Technology
https://www.journals.elsevier.com/journal-of-materials-research-and-technology

Original Article

The effect of *Impatiens balsamina* L. extract on structural, morphological, optical, and photocatalytic properties of Zn_2SnO_4

Eka Angasa [a,b], *Asdim* [a,b], *Zulhadjri* [a], *Novesar Jamarun* [a], *Syukri Arief* [a,*]

[a] *Materials Laboratory, Department of Chemistry, Andalas University, Padang, Indonesia*
[b] *Department of Chemistry, Bengkulu University, Bengkulu, Indonesia*

ARTICLE INFO

Article history:
Received 14 July 2020
Accepted 2 September 2020
Available online 24 September 2020

Keywords:
Zn_2SnO_4
Impatiens balsamina L.
Photocatalyst
Methylene blue

ABSTRACT

In this study, a facile and green synthesis approach of Zn_2SnO_4 was conducted by using *Impatiens balsamina* L. aqueous leaf extract through the hydrothermal method. The results show that Zn_2SnO_4 was successfully produced with a specific characteristic which is strongly influenced by the presence of extract. Furthermore, X-ray diffraction (XRD) pattern showed an enhancement of crystallinity along with the increase of extract quantity. Scanning electron microscope (SEM) and transmission electron microscope (TEM) analysis confirmed the formation of irregular, spherical, and octahedral shaped of Zn_2SnO_4 particles, based on extract concentration used. The optical bandgap values of the obtained Zn_2SnO_4 were different based on morphology. This is because the synthesized microstructure showed good photocatalytic activity in the degradation of methylene blue (MB) under UV irradiation. These results confirm that *I. balsamina* is a promising material for mediating the synthesis of Zn_2SnO_4, the properties of which can be controlled by adjusting the concentration of the leaf extract.

1. Introduction

Presently, photolysis is considered as an effective and sustainable way to restore the polluted environment. Zn_2SnO_4 as a significant n-type ternary metal oxide semiconductor is one of the most attractive materials with the extensive application. This is due to the excellent properties such as high electron mobility ($10-15\ cm^2\ V^{-1}\ s^{-1}$), wide bandgap (3.6 eV), high electrical conductivity ($\sim 10^4\ Scm^{-1}$), low visible absorption, and unique optical properties [1–4]. It has been widely used as photocatalyst [3,5], solar cells [6,7], gas sensors [8,9], and anode in Li-ion batteries [10,11].

It is well known that the performance of materials is driven by physicochemical and optoelectronic properties [12]. Therefore, it is necessary to determine the morphology and size of Zn_2SnO_4 nanoparticles as the most important factor determining these properties. Some additives can be utilized in the synthesis process to achieve this morphology and size. It was reported that the addition of CTAB and L-tryptophan in the reactions resulted in octahedral micro-structured of Zn_2SnO_4 with nano-plate hexagon [13,14]. In addition, the use of carbohydrate sugars in the reaction resulted in the Zn_2SnO_4 nanostructure [15]. Likewise, the micro-octahedral

* *Corresponding author.*
E-mail: syukriarief@sci.unand.ac.id (S. Arief).

https://doi.org/10.1016/j.jmrt.2020.09.017

Zn_2SnO_4 showed an improvement in photocatalytic activity, which resulted in a high capacity to convert CO_2 to CH_4 [13].

However, the production of nanoparticles has a high potential for environmental damage due to the use of hazardous chemicals and may affect bio-application in the future. Hence, it is necessary to use a green synthesis method using non-hazardous chemicals. Plant extracts have received a lot of attention due to the ability to act as a capping and reducing agent [16,17]. They contain some bioactive compounds such as terpenoids, flavonoids, aldehydes, amides, ketones, and carboxylic acids, which can reduce the metal ions to form nanoparticles. Furthermore, they act as stabilizing agent by occurring chelate interaction with nanoparticles [18]. This makes it possible to produce stable nanoparticles of different sizes, and in addition, it is easy, safe, and low cost and energy required [17,19,20]. We focus on the exploration of plant extracts in synthesis of metal/metal oxide which enhance their performance. Previously, we employed *Garcinia mangostana* fruit peel extract to prepare octahedral Zn_2SnO_4 [21].

This study investigated the use of *Impatiens balsamina* leaf extract for synthesizing controlled Zn_2SnO_4. *I. balsamina* leaf extract contains some powerful active compounds such as lawsone, bilowsone, lawsone methyl ether, phenolic, and flavonoids which actively chelate metal ion as well as reduce it into nanoparticles with varying characteristics [22–25]. Aritonang et al. and Roy et al. reported that the leaf extract of *I. balsamina* is used as both reducing and stabilizing agents in the preparation of silver and copper nanoparticles, respectively [26,27]. To the best of our knowledge, this report is the first to study the use of *I. balsamina* L. leaf extract in the synthesis of Zn_2SnO_4. It was discovered that the extract had a strong effect on the size, morphologies, crystallinity, and optical properties of the resulting Zn_2SnO_4. In addition, the photocatalytic activity was also studied through methylene blue degradation.

2. Material and methods

2.1. Synthesis of Zn_2SnO_4

All reagents used in the experiment were of analytical grade quality without further purification. Zinc acetate dihydrate ($Zn(CH_3COO)_2.2H_2O$, purity ≥99,5%) and sodium hydroxide (NaOH) were purchased from Merck. Furthermore, Tin (IV) Chloride ($SnCl_4$, purity 98%) was purchased from Sigma Aldrich, and fresh leaves of the used plant were collected from the flower garden at Khatib Sulaiman Street, Padang, Indonesia.

Fresh *I. balsamina* leaves were washed with tap and demineralized water (DM-aqua) before been cut into small pieces. It was then transferred into a 100 mL flask and added by DM-aqua. The mixture was stirred in room temperature for 30 min, followed by filtration using Hyndai filter paper No. 10.

Zn_2SnO_4 was prepared using hydrothermal method as reported in Ref. [21]. 10 mL of 0.2 M $Zn(CH_3COO)_2.H_2O$ was added into 10 mL of 0.1 M $SnCl_4$ and stirred at room temperature. After a 10-minute reaction, the mixed solution was gradually added by 5 mL of balsam leaf extract. Then, 20 mL of 0.4 M NaOH solution was added into the reaction and was stirred for 30 min. Furthermore, the obtained white suspension with a total volume of 45 mL was transferred into a 100 mL of Teflon lined stainless steel hydrothermal autoclave. It was heated at a temperature of 185 °C for 18 h and was allowed to cool after the reaction. The as-synthesized sample was filtered using Whatman filter paper No. 42, washed using DM-aqua, and the final product was dried in a hot-air oven at a temperature of 85 °C for 16 h. To investigate the effect of the extract on the properties of the product, the extract concentration was varied to be 2, 4, 6, 8, 10, 12, and 14%. In addition, the ratio of starting materials OH: Zn^{+2}: Sn^{+4} was variated to be 7:2:1, 8:2:1, 9:2:1, 10:2:1, 11:2:1 as well.

2.2. Characterization

The crystal structure and phase of the samples were measured by XRD with Cu Kα radiation (λ = 1.5406 Å). The morphology and size of samples were observed by SEM (FEI (Inspect-S50)) and TEM (JEM-1400). Also, a UV–vis DRS analysis (Analytik Jena) was conducted to evaluate the optical absorption spectrum of samples.

2.3. Examination of photocatalytic performance

The photocatalytic performance of synthesized Zn_2SnO_4 was investigated through the degradation of MB solution at room temperature. The experiment was conducted in different conditions, i.e. (a) without catalyst under irradiation of UV light (blank), (b) with catalyst in dark condition, and (c) with the catalyst under irradiation of UV light. 50 mg of prepared Zn_2SnO_4 was suspended into 100 mL of 20 mg L^{-1} MB and stirred in dark condition for 30 min before irradiation to establish adsorption-desorption equilibrium. Furthermore, the suspensions were irradiated with a 30 W UV lamp. An aliquot of the samples was withdrawn, centrifuged, and measured using a T70 UV–vis spectrophotometer. All data were reported as mean ± standard deviation, collected by triplicate experiment. A one way ANOVA test was used to determine the significance of photodegradation efficiencies of prepared Zn_2SnO_4 using the Analysis Toolpak Program of Microsoft Excel.

3. Results and discussion

3.1. Sample and characterization

XRD pattern of the samples prepared using *I. balsamina* leaf extract is shown in Fig. 1. It was observed that the quantity of extract in the reaction affects the crystal structure and phase composition of the sample. In the use of 2% extract, 3 crystal phases were formed i.e. ZnO with the highest, and Zn_2SnO_4, as well as SnO_2 with the lowest intensities. Conversely, in the use of a 4% extract, a single phase of Zn_2SnO_4 was observed. It was specifically referred to inverse cubic spinel structure Zn_2SnO_4 based on JCPDS 024-1470 standard. The intensity of the peaks was increased along with the rise of extract concentration up to 10%, indicating an increase in crystallinity. These results demonstrate a high purity of the synthesized Zn_2SnO_4. Finally, no Zn_2SnO_4 peak was observed while using 14% of the extract. It means that in a certain concentration,

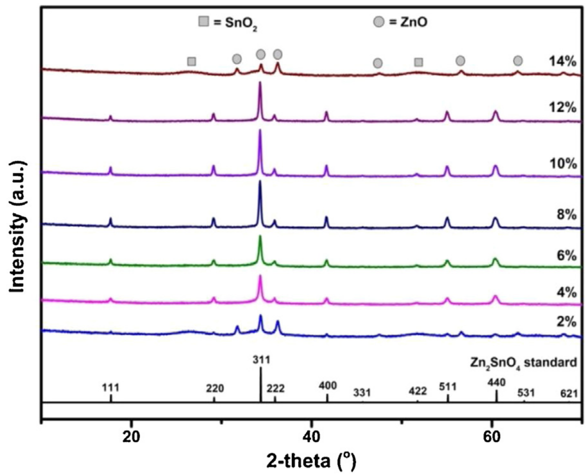

Fig. 1 – XRD patterns of product with variation of extract.

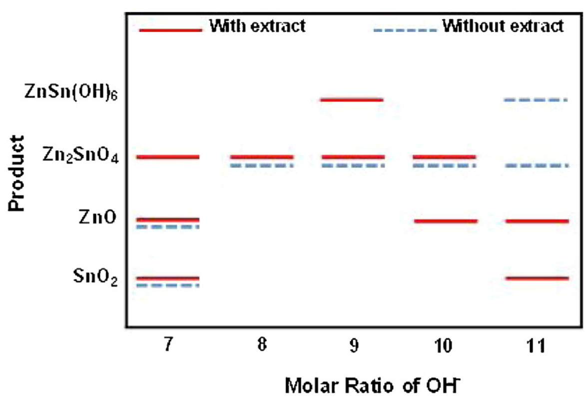

Fig. 2 – Phase change diagram of as-synthesized product with variation of OH⁻ molar ratio with and without extract.

I. balsamina leaf extract plays an important role in enhancing the crystallinity and phase of synthesized Zn_2SnO_4. The biomolecules of extract were actively involved during nucleation, growth, and stabilization process of Zn_2SnO_4 particles, resulting in a high crystallinity [18]. Following this result, the optimum extract concentration resulting in single-phase Zn_2SnO_4 with high crystallinity was 8%. Therefore, this concentration is used in the synthesis with a variation of alkali ratio.

Furthermore, the effect of the extract was investigated in a varied amount of alkali on the crystal phase of prepared Zn_2SnO_4 (Fig. 2). It was observed that in the presence of extract, Zn_2SnO_4 is formed at the OH^- ratio of 7 along with the formation of ZnO and SnO_2. By the rise of alkali in a ratio of 8, a single phase of Zn_2SnO_4 was observed. However, in the addition of alkali with a ratio of 9 and 10, Zn_2SnO_4 was formed along with other phases i.e. $ZnSn(OH)_6$ and ZnO. In the use of alkali with a ratio of 11, Zn_2SnO_4 was not formed. A Contrast appearance was observed in the samples prepared without using extract, and a single-phase Zn_2SnO_4 was formed in the use of OH^- ratio of 8, 9, and 10. Furthermore, $ZnSn(OH)_6$ was formed in the OH^- ratio of 11, and it quickly appeared in the synthesis process as an intermediate and metastable phase. However, it can be decomposed and continuously crystallized during the hydrothermal process to form Zn_2SnO_4 [14,28]. However, due to the excessive amount of alkali, $ZnSn(OH)_6$ is formed as the final product in pH above 10 [29]. By the different results of the experiment with and without extract, it was confirmed that *I. balsamina* leaf extract initiates a rapid formation of $ZnSn(OH)_6$. This initiation may be due to interactions between metal ions of precursor and oxygen atoms of extract compound's functional group or released by the degradation process [18,30].

SEM and TEM analysis were conducted to investigate the effect of *I. balsamina* leaf extract on the morphology of Zn_2SnO_4. The SEM micrograph of the samples is displayed in Fig. 3. It was shown that by the use of 4 and 6% leaf extract, the particles were agglomerated in irregular shape (Fig. 3a,b). Furthermore, when the concentration of the extract was raised to 8 and 10%, the particles were aggregated and well-dispersed. Most of the particles were octahedral in shape with a size length of 0.16–0.35 μm (Fig. 3c–e). However, the increase of the extract concentration to 12% leads to a formation of like-spherical particles and tends to agglomerated (Fig. 3f). This result confirmed that the use of *I. balsamina* leaf extract with a concentration of 8–10% can effectively act as a capping agent in the synthesis process of Zn_2SnO_4. In addition, octahedral and spherical-like shaped particles were confirmed by TEM analysis as shown in Fig. 4. Tetragonal shape as shown in Fig. 4a confirmed that the particles were projected by focusing the electron beam on one of the vertex angles along the [001] direction of octahedron [13]. Also, the result showed that all the particles formed in the synthesis process of Zn_2SnO_4 without extract were agglomerated and irregular in shape as previously reported (Fig. S1) [21]. This result showed that *I. balsamina* leaf extract played an essential role in controlling the formation of Zn_2SnO_4 particles.

A more regular shape of octahedral Zn_2SnO_4 particles was obtained using an OH^- molar ratio of 9 (Fig. 5a). However, it was shown that the particle size was greater than those synthesized with OH^- having a molar ratio of 8 (0.28–0.65 μm). TEM images of octahedral Zn_2SnO_4 were displayed in Fig. 5b. Furthermore, the hexagonal shape also indicates the formation of octahedron [13]. Unlikely, the micrograph of the sample synthesized in lower and higher OH- molar ratio of 9 showed the formation of agglomerated and irregular shape since no octahedron particle was observed (Fig. S2).

The actual mechanism of the formation of octahedral Zn_2SnO_4 particles mediated by plant extract was not discovered. However, literature suggests that active compounds in the plant extract contribute to the faster crystal growth in the plane of [100] than those of [111] [13,31]. Following the Zn_2SnO_4 crystal model, [111] plane has a more positive charge caused by the presence of un-saturated Zn and Sn atoms with dangling bonds. Therefore, active functional groups such as hydroxyl and ketone in *I. balsamina* extract may act as ligand and form a selective bond with Zn^{+2} and Sn^{+4} ions. It helps to slacken the nucleation and growth process along the [111] plane but rapid ones in [100], causing the formation of octahedron particles [13]. An illustration of the possible mechanisms of octahedral Zn_2SnO_4 formation was shown in Fig. 6.

The optical properties of as-synthesized Zn_2SnO_4 were determined using UV–vis DRS (Fig. 7). Fig. 7a shows the UV–vis

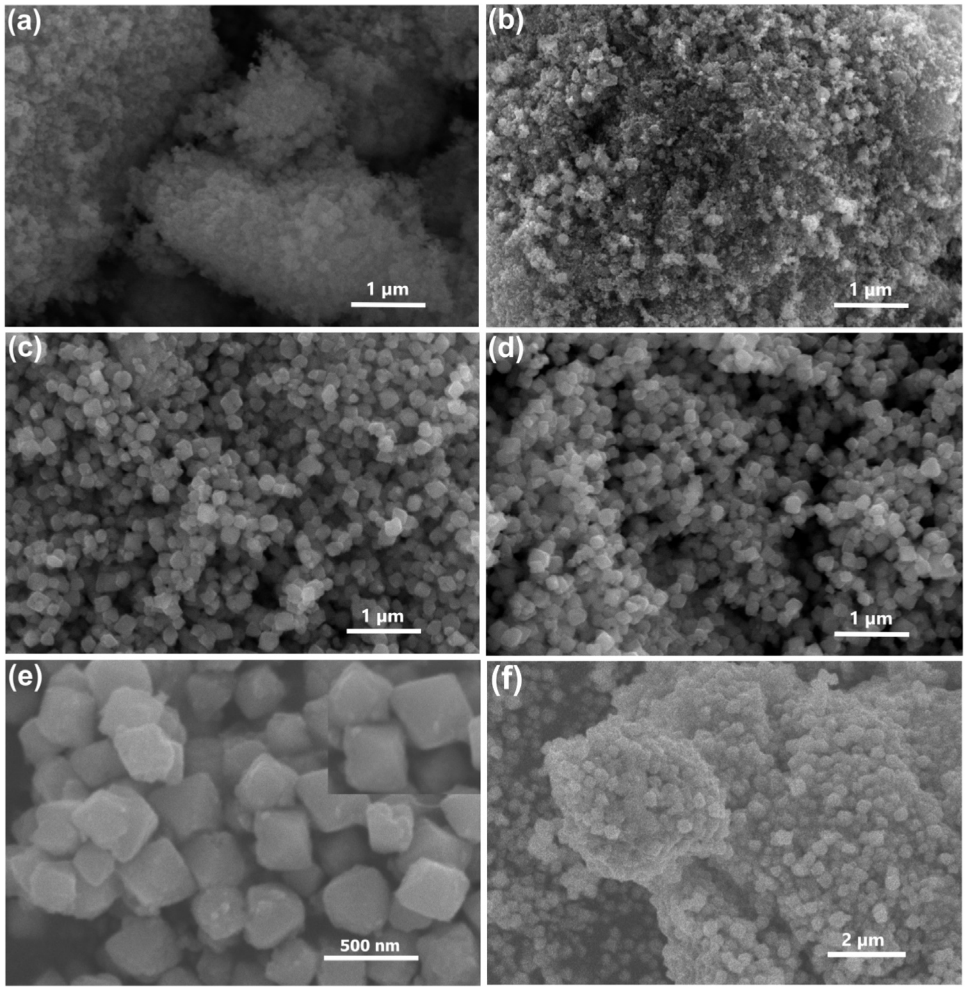

Fig. 3 – SEM and TEM images of Zn_2SnO_4 with extract concentration, (a) 4%, (b) 6%, (c) 8%, (d) 10%, (e) 8% in higher resolution, and (f) 12%.

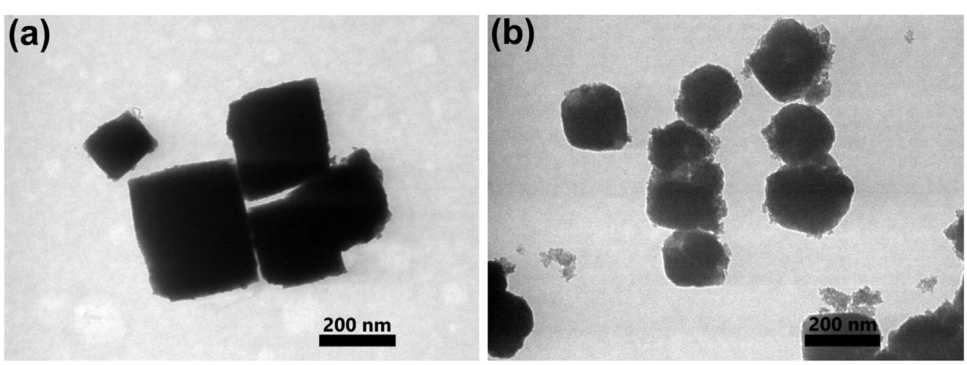

Fig. 4 – TEM images of Zn_2SnO_4 prepared using extract, (a) 8% and (b) 12%.

spectrum of Zn_2SnO_4 in the variation of extract concentration. The steep peak is shown in all spectra, indicating that the absorbance is from the bandgap transition of the samples instead of the impurity level. It is observed that all samples exhibit absorbance at different wavelengths due to the adjustment of the mean grain size of the samples, caused by the presence of *I. balsamina* leaf extract [32]. The maximum absorbance was obtained using a 4% extract indicating the lowest optical bandgap (E_g), while the minimum was obtained using 10% extract. Also, the Tauc's Formula ($(\alpha h\upsilon)^{1/n} = (h\upsilon\text{-}E_g)$) was used to estimate the optical bandgap of prepared Zn_2SnO_4 [33]. As direct transition (n = 1/2), it is determined by plotting linear portion to the energy axis in zero absorption of $(\alpha h\upsilon)^2$ versus $h\upsilon$ curve [34]. The bandgap value of the samples prepared using 4, 6, 8, 10, and 12% extract were 3.47, 3.49, 3.53, 3.54, and 3.51, respectively, as shown in Fig. 7b. It was observed

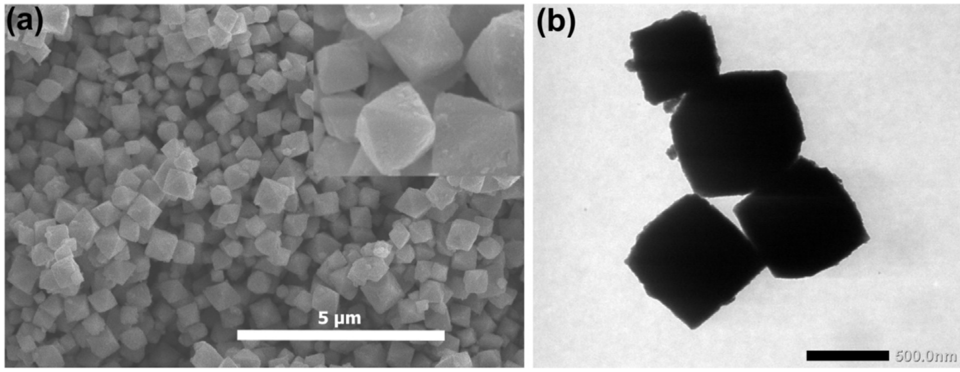

Fig. 5 – SEM and TEM images of Zn_2SnO_4 with OH^- molar ratio of 9 in present 8% of extract.

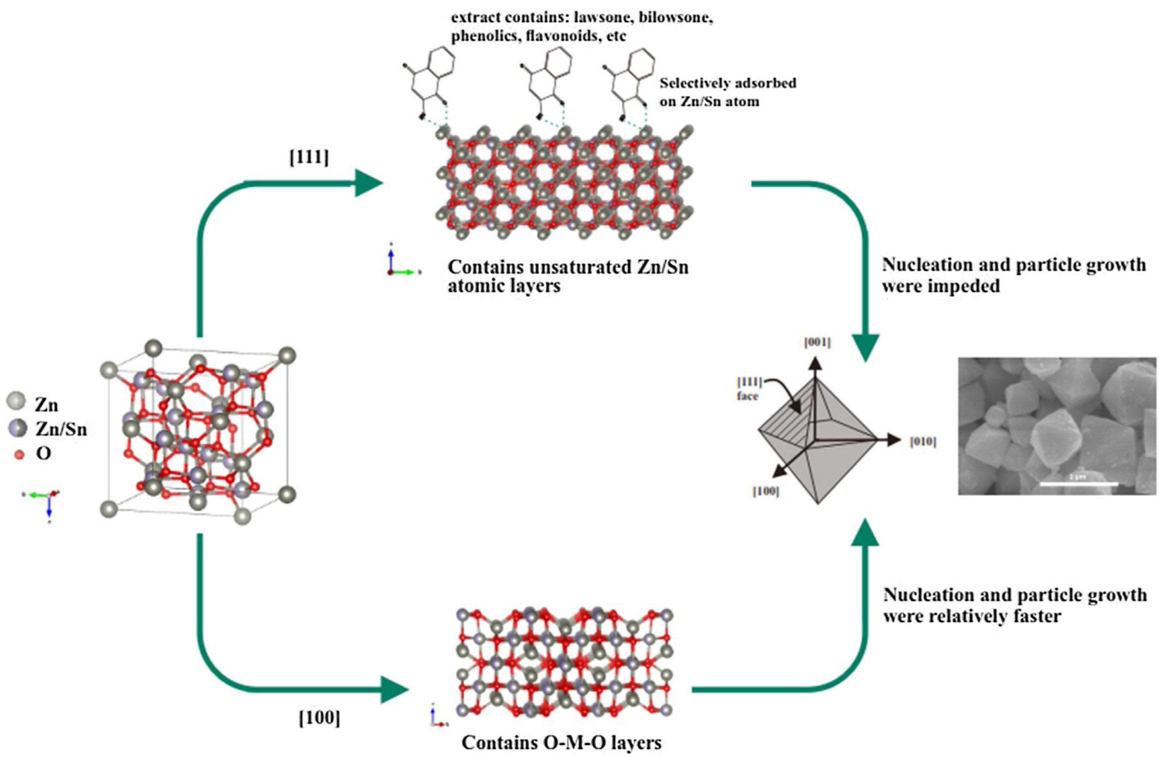

Fig. 6 – Illustrative scheme of possible mechanisms of octahedral Zn_2SnO_4 formation using *I. balsamina* leaf extract.

that the bandgap value was gradually increased using 10% extract and then decrease using 12%. The difference in size and morphology of Zn_2SnO_4 have a significant effect on their bandgap values [15,35]. In addition, the sample prepared by 8 and 10% extract was regular in shape without any agglomeration particles formed and has the highest bandgap value. Conversely, the sample prepared with 12% extract was regular in shape but agglomerated, and has a lower bandgap value. However, E_g of all samples are slightly lower than bulk Zn_2SnO_4 (3.6 eV), and it is related to the incorporation of excess Zn, which caused heat treatment during synthesis [32].

3.2. *Photocatalytic performance*

The photocatalytic performance of Zn_2SnO_4 prepared with the variation of extract concentration was evaluated through photodegradation of methylene blue (MB) under UV light. The temporal evolution of MB time-dependent absorption was conducted in the presence of Zn_2SnO_4 using an 8% extract (shown in Fig. 8a). Furthermore, the specific absorbance peak was provided in a wavelength of around 664 nm. It was observed that the intensity was rapidly decreased during UV light irradiation, indicating a good photocatalytic activity. After 75 min of irradiation, the MB absorption peak almost disappeared and remained constant up to 90 min. Fig. 8b displays a concentration change of solution during the irradiation time interval, where C_0 refers to initial concentration, while C refers to the actual. It is observed that a very low degradation of MB was shown in the dark condition and the absence of the catalyst (blank). This shows that the octahedral Zn_2SnO_4 plays a strong role in the degradation of MB under UV light.

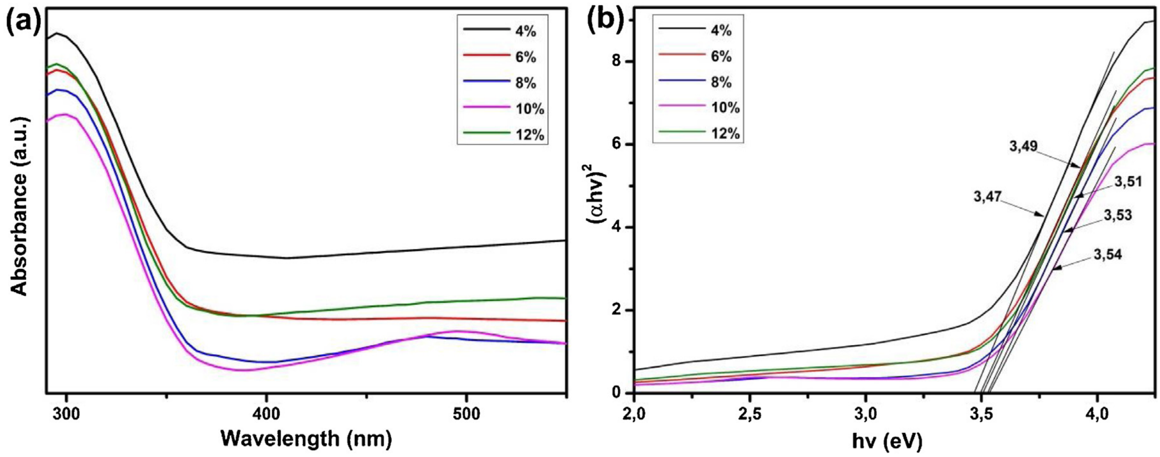

Fig. 7 – (a) The UV–vis absorption spectra of prepared Zn_2SnO_4, (b) plot curve of $(\alpha h\upsilon)^2$ versus $h\upsilon$.

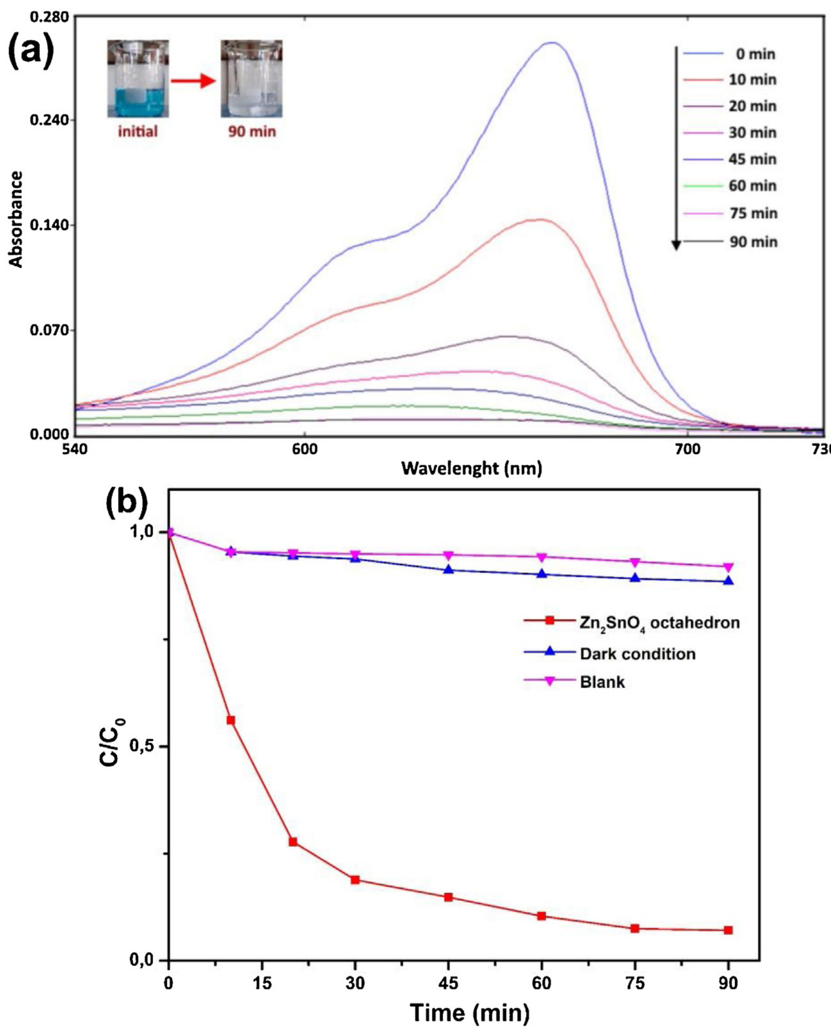

Fig. 8 – (a) Time-dependent photodegradation spectra of MB using Zn_2SnO_4 prepared of 8% extract, (b) degradation rate of MB as an irradiation time function in different condition.

The degradation efficiency of MB after 90 min of reaction showed that the extract concentration significantly influenced the efficiency ($p < 0.05$), as observed in Fig. 9. It is shown that the highest degradation efficiency was obtained using 8 and 10% extract with a value of 92.92 and 94.9%, respectively. In addition, the degradation efficiencies are higher than Zn_2SnO_4 prepared using mangosteen fruit peel extract and without extract, i.e. 85.94 and 78.93%, respectively [21].

Table 1 – Characteristics and degradation efficiencies of synthesized Zn_2SnO_4 with different extract concentration.

No	Sample with Extract Variation (%)	Morphology	Particle Size (μm)	Band Gap (eV)	Degradation Efficiency (%)
1	4	Agglomerated and irregular	–	3.47	89.43 ± 1.25
2	6	Agglomerated and irregular	–	3.49	90.32 ± 1.04
3	8	Octahedral	0.16–0.35	3.53	92.92 ± 1.08
4	10	Octahedral	0.16–0.27	3.54	94.90 ± 1.54
5	12	Spherical-like	0.14–0.25	3.51	92.09 ± 0.87

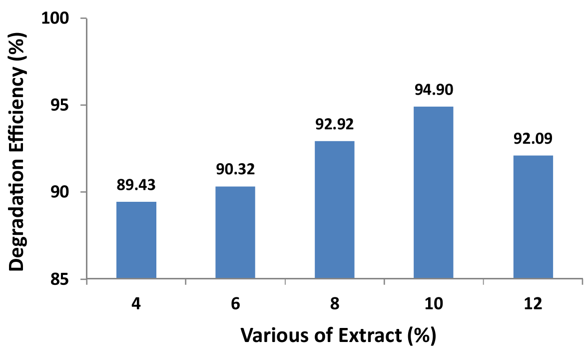

Fig. 9 – Degradation efficiency of synthesized Zn_2SnO_4 with different extract concentration.

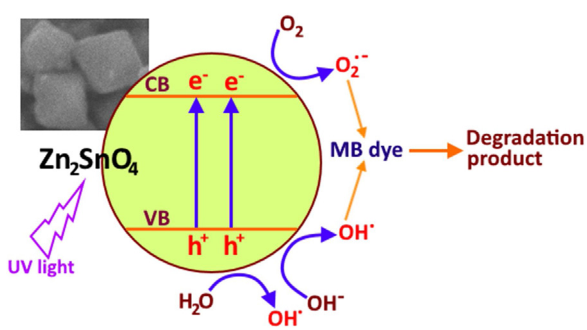

Fig. 10 – Schematic diagram of photodegradation mechanism of MB using Zn_2SnO_4.

The photodegradation mechanism of MB using Zn_2SnO_4 is illustrated in Fig. 10. When UV light irradiated the Zn_2SnO_4 surface, electrons (e^-) and holes (h^+) are generated. Then, h^+ is entangled by OH^- ions or H_2O molecules at the Zn_2SnO_4 surface to form hydroxyl radicals (·OH). Meanwhile, e^- are entangled by O_2 molecules to yield superoxide radical anions ($\cdot O_2^-$). These resulting radicals are very strong oxidizing agents that can effectively decompose MB molecules [34,36,37]. These radical formations depend on the adsorption efficiency of H_2O, OH^-, and O_2 on Zn_2SnO_4 surface as well as the longer separation of e^- and h^+ after irradiation. Therefore, the improvement of morphology and crystallinity of Zn_2SnO_4 are key factors in increasing photodegradation of MB. The samples prepared using extract of 8 and 10% result in well aggregated faceted octahedral particles with the highest degradation efficiency as shown in Table 1. Also, the presence of extract improves the morphology and crystallinity of Zn_2SnO_4 that enhance photocatalytic activity in the degradation of MB.

4. Conclusion

An eco-friendly hydrothermal method was used to prepare Zn_2SnO_4 using *I. balsamina* leaf extract. It was used to modify and control the crystallinity, morphology, size, and optical properties of Zn_2SnO_4. XRD analysis confirms the formation of the inverse cubic spinel structure of Zn_2SnO_4, where the crystallinity of the samples was strongly influenced by the concentration of the extract. The single-phase with the highest crystallinity was obtained by using 8% extract. SEM and TEM analysis results showed that by using 8 and 10% extract, octahedral shaped particles were formed with a side length of 0.16–0.35 μm. Meanwhile, the highest photodegradation efficiency was obtained using 10% of the extract. The photocatalytic activity was increased using 8% and 10% extract due to the better morphology, size, crystallinity, and bandgap of the samples. A significant correlation between extract concentration, shape, and photocatalytic activity was observed. Furthermore, a study on the actual mechanism of *I. balsamina* leaf extract needs to be conducted since it controls the growth and aggregation of the particles. This study confirmed that *I. balsamina* is one of the promising and eco-friendly resources to prepared and modify the properties of metal/oxide-metal nanoparticles.

Conflicts of interest

The authors declare no conflicts of interest.

Acknowledgements

This work was supported by the Ministry of Finance Indonesia through Lembaga Pengelola Dana Pendidikan (LPDP) [grant number PRJ-6090/LPDP.3/2016].

Appendix A. Supplementary data

Supplementary material related to this article can be found, in the online version, at doi:https://doi.org/10.1016/j.jmrt.2020.09.017.

REFERENCES

[1] Shi L, Dai Y. Synthesis and photocatalytic activity of Zn2SnO4 nanotube arrays. J Mater Chem A 2013;1:12981–6, http://dx.doi.org/10.1039/c3ta12388j.

[2] Al-Attafi K, Jawdat FH, Qutaish H, Hayes P, Al-keisy A, Shim K, et al. Cubic aggregates of Zn2SnO4 nanoparticles and their application in dye-sensitized solar cells. Nano Energy 2019;57:202–13, http://dx.doi.org/10.1016/j.nanoen.2018.12.039.
[3] Fakhrzad M, Navidpour AH, Tahari M, Abbasi S. Synthesis of Zn2SnO4 nanoparticles used for photocatalytic purposes. Mater Res Express 2019;6, http://dx.doi.org/10.1088/2053-1591/ab2eb5.
[4] Hwang D, Jin JS, Lee H, Kim HJ, Chung H, Kim DY, et al. Hierarchically structured Zn2SnO4 nanobeads for high-efficiency dye-sensitized solar cells. Sci Rep 2014;4, http://dx.doi.org/10.1038/srep07353.
[5] Das PP, Roy A, Tathavadekar M, Devi PS. Photovoltaic and photocatalytic performance of electrospun Zn2SnO4. Appl Catal B Environ 2017;203:692–703, http://dx.doi.org/10.1016/j.apcatb.2016.10.035.
[6] Dou J, Li X, Li Y, Chen Y, Wei M. Fabrication of Zn2SnO4 microspheres with controllable shell numbers for highly efficient dye-sensitized solar cells. Sol Energy 2019;181:424–9, http://dx.doi.org/10.1016/j.solener.2019.02.016.
[7] Das PP, Roy A, Agarkar S, Devi PS. Hydrothermally synthesized fluorescent Zn2SnO4 nanoparticles for dye sensitized solar cells. Dyes Pigm 2018;154:303–13, http://dx.doi.org/10.1016/j.dyepig.2017.12.066.
[8] Xu T-T, Xu Y-M, Zhang X-F, Deng Z-P, Huo L-H, Gao S. Enhanced H2S gas-sensing performance of Zn2SnO4 lamellar micro-spheres. Front Chem 2018;6:1–5, http://dx.doi.org/10.3389/fchem.2018.00165.
[9] Thanh HX, Trung DD, Trung KQ, Van Dam K, Van Duy N, Hung CM, et al. On-chip growth of single phase Zn2SnO4 nanowires by thermal evaporation method for gas sensor application. J Alloys Compd 2017;708:470–5, http://dx.doi.org/10.1016/j.jallcom.2017.03.014.
[10] Xia J, Tian R, Guo Y, Du Q, Dong W, Guo R, et al. Zn2SnO4-carbon cloth freestanding flexible anodes for high-performance lithium-ion batteries. Mater Des 2018;156:272–7, http://dx.doi.org/10.1016/j.matdes.2018.06.056.
[11] Zhang R, He Y, Xu L. Controllable synthesis of hierarchical ZnSn(OH)6 and Zn2SnO4 hollow nanospheres and their applications as anodes for lithium ion batteries. J Mater Chem A 2014, http://dx.doi.org/10.1039/b000000x.
[12] Nunez J, Fresno F, Collado L, Jana P, Coronado JM, Serrano DP, et al. Photocatalytic H2 production from aqueous methanol solutions using metal-co-catalysed Zn2SnO4 nanostructures. Appl Catal B Environ 2016;191:106–15, http://dx.doi.org/10.1016/j.apcatb.2016.03.020.
[13] Li Z, Zhou Y, Zhang J, Tu W, Liu Q, Yu T, et al. Hexagonal nanoplate-textured micro-octahedron Zn2SnO4: combined effects toward enhanced efficiencies of dye-sensitized solar cell and photoreduction of CO2 into hydrocarbon fuels. Cryst Growth Des 2012;12:1476–81, http://dx.doi.org/10.1021/cg201568q.
[14] Ji X, Huang X, Liu J, Jiang J, Li X, Ding R, et al. Hydrothermal synthesis of novel Zn2SnO4 octahedron microstructures assembled with hexagon nanoplates. J Alloys Compd 2010;503:L21–5, http://dx.doi.org/10.1016/j.jallcom.2009.12.038.
[15] Masjedi-Arani M, Salavati-Niasari M. Effect of carbohydrate sugars as a capping agent on the size and morphology of pure Zn2SnO4 nanostructures and their optical properties. Mater Lett 2016;174:71–4, http://dx.doi.org/10.1016/j.matlet.2016.03.084.
[16] Kalpana VN, Rajeswari VD. A Review on green synthesis, biomedical applications, and toxicity studies of ZnO NPs. Bioinorg Chem Appl 2018;ID 3569758:1–12, http://dx.doi.org/10.1155/2018/3569758.
[17] El-seedi HR, El-shabasy RM, Khalifa SAM, Saeed A, Shah A, Shah R, et al. Metal nanoparticles fabricated by green chemistry using natural extracts: biosynthesis, mechanisms, and applications. RSC Adv 2019;9:24539–59, http://dx.doi.org/10.1039/c9ra02225b.
[18] Jeevanandam J, Chan YS, Danquah MK. Biosynthesis of metal and metal oxide nanoparticles. ChemBioEng Rev 2016;3:55–67, http://dx.doi.org/10.1002/cben.201500018.
[19] Matussin S, Harunsani MH, Tan AL, Khan MM. Plant extract-mediated SnO2 nanoparticles: synthesis and applications. ACS Sustain Chem Eng 2020;8(8):3040–54 https://doi.org/10.1021/acssuschemeng.9b06398.
[20] Iravani S. Green synthesis of metal nanoparticles using plants. Green Chem 2011;13:2638, http://dx.doi.org/10.1039/c1gc15386b.
[21] Angasa E, Putri YE, Zulhadjri, Jamarun N, Arief S. Improving the morphological, optical, and photocatalytic properties of octahedral Zn2SnO4 using Garcinia mangostana fruit peel extract. Vacuum 2020;182:109719.
[22] Clevenger S. The flavonols of Impatiens balsamina L. Arch Biochem Biophys 1958;76:131–8.
[23] Bohm BA, Towers GHN. A study of phenolic compounds in impatiens. Can J Bot 1962;40.
[24] Yang X, Summerhurst DK, Koval SF, Ficker C, Smith ML, Bernards MA. Isolation of an antimicrobial compound from Impatiens balsamina L. using bioassay-guided fractionation. Phyther Res 2001;15:676–80, http://dx.doi.org/10.1002/ptr.906.
[25] Makarov VV, Love AJ, Sinitsyna OV, Makarova SS, Yaminsky IV, Taliansky ME, et al. Green nanotechnologies: synthesis of metal nanoparticles using plants. Acta Naturae 2014;6:35–44, http://dx.doi.org/10.1039/c1gc15386b.
[26] Aritonang HF, Koleangan H, Wuntu AD. Synthesis of silver nanoparticles using aqueous extract of medicinal plants' (Impatiens balsamina and Lantana camara) fresh leaves and analysis of antimicrobial activity. Int J Microbiol 2019;2019, http://dx.doi.org/10.1155/2019/8642303.
[27] Roy K, Ghosh CK, Sarkar CK. Degradation of toxic textile dyes and detection of hazardous Hg2+ by low-cost bioengineered copper nanoparticles synthesized using Impatiens balsamina leaf extract. Mater Res Bull 2017, http://dx.doi.org/10.1016/j.materresbull.2017.06.016.
[28] Firooz AA, Mahjoub AR, Khodadadi AA, Movahedi M. High photocatalytic activity of Zn2SnO4 among various nanostructures of Zn2xSn1−xO2 prepared by a hydrothermal method. Chem Eng J 2010;165:735–9, http://dx.doi.org/10.1016/j.cej.2010.09.052.
[29] Sun G, Zhang S, Li Y. Solvothermal synthesis of Zn2SnO4 nanocrystals and their photocatalytic properties. Int J Photoenergy 2014;580615:1–7, http://dx.doi.org/10.1155/2014/580615.
[30] Khalafi T, Buazar F, Ghanemi K. Phycosynthesis and enhanced photocatalytic activity of zinc oxide nanoparticles toward organosulfur pollutants. Sci Rep 2019;9:1–10, http://dx.doi.org/10.1038/s41598-019-43368-3.
[31] Miyauchi M, Liu Z, Zhao ZG, Anandan S, Hara K. Single crystalline zinc stannate nanoparticles for efficient photo-electrochemical devices. Chem Commun 2010;46:1529–31, http://dx.doi.org/10.1039/b921010e.
[32] Alpuche-Aviles MA, Wu Y. Photoelectrochemical study of the band structure of Zn2SnO4 prepared by the hydrothermal method. J Am Chem Soc 2009;131:3216–24, http://dx.doi.org/10.1021/ja806719x.
[33] Wood DL. Weak absorption tails in amorphous semiconductors. Phys Rev B 1972;5:3144–51, http://dx.doi.org/10.1103/PhysRevB.5.3144.
[34] Zeng J, Xin M, Li K, Wang H, Yan H, Zhang W. Transformation process and photocatalytic activities of hydrothermally

synthesized. J Phys Chem C 2008;112:4159–67, http://dx.doi.org/10.1021/jp7113797.
[35] Hidalgo MC, Aguilar M, Maicu M, Navío JA, Colón G. Hydrothermal preparation of highly photoactive TiO2 nanoparticles. Catal Today 2007;129:50–8, http://dx.doi.org/10.1016/j.cattod.2007.06.053.
[36] Zhao Q, Deng X, Ding M, Huang J, Ju D, Xu X. Synthesis of hollow cubic Zn2SnO4sub-microstructures with enhanced photocatalytic performance. J Alloys Compd 2016;671:328–33, http://dx.doi.org/10.1016/j.jallcom.2016.01.264.
[37] Testino A, Bellobono IR, Buscaglia V, Canevali C, Arienzo MD, Polizzi S, et al. Optimizing the photocatalytic properties of hydrothermal TiO2 by the control of phase composition and particle morphology. A systematic approach. J Am Chem Soc 2007;129:3564–75, http://dx.doi.org/10.1021/ja067050+.